Nanoscale

PAPER

View Article Online
View Journal | View Issue

Cite this: *Nanoscale*, 2016, **8**, 19867

Near-field Raman dichroism of azo-polymers exposed to nanoscale dc electrical and optical poling

Sergey S. Kharintsev,*[a,b] Alexandr I. Fishman,[a] Semion K. Saikin[c,d] and Sergei G. Kazarian[e]

Received 22nd September 2016,
Accepted 4th November 2016

DOI: 10.1039/c6nr07508h

www.rsc.org/nanoscale

Azobenzene-functionalized polymer films are functional materials, where the (planar *vs.* homeotropic) orientation of azo-dyes can be used for storing data. In order to characterize the nanoscale 3D orientation of the pigments in sub-10 nm thick polymer films we use two complementary techniques: polarization-controlled tip-enhanced Raman scattering (TERS) microscopy and contact scanning capacity microscopy. We demonstrate that the homeotropic and planar orientations of the azo-dyes are produced by applying a local dc electrical field and a resonant longitudinal optical near-field, respectively. For a non-destructive probe of the azo-dye orientation we apply a non-resonant optical near-field and compare the intensities of the Raman-active vibrational modes. We show that near-field Raman dichroism, a characteristic similar to the absorption dichroism used in far-field optics, can be a quantitative indicator of the 3D molecular orientation of the azo-dye at the nanoscale. This study directly benefits the further development of photochromic near-field optical memory that can lead to ultrahigh density information storage.

1. Introduction

The well-established properties of light at the nanoscale empower us to use it in a wide range of applications, including optical switching and storage[1–3] operating on the same principles as phase change semiconductor memory.[4] However, diffraction-limited optics are able to record as much information as ~1 Gb in^{-2}. Non-linear optical effects, for example, two-photon fluorescence recording,[5] allow one to increase the recording density up to ~100 Gb in^{-2}. Going beyond the diffraction limit, due to light localization, pushes the minimal storage extent down to a single chromophore of ~1 nm in length. Thus, the memory capacity can be potentially increased up to the theoretical limit of ~1 Pb in^{-2}. Moreover, as compared to diffraction-limited optics, the electromagnetic field confinement provides faster recording and read-out operations due to the enhanced light–matter interaction. A short-range character of optical near-fields leads to photochromic films with a thickness of ~10 nm or less, rather than bulk polymers.

Controlling the transverse and longitudinal diffraction-free optical anisotropy in photo-responsive organic solid materials is an ongoing challenge.[6] Considerable progress in polarization-controlled diffraction-limited optical microscopy has been achieved due to the longitudinal *z*-polarization of focused laser beams.[7–11] The simplest case is related to highly squeezed (NA > 1) linearly polarized light, for which the z-component of an electric field exceeds the transverse component by four times at NA = 1.49.[12] In practice, this approach is of little use because of mixed polarization; the focused light contains both (*xy*) transverse and (*z*) longitudinal polarization which are spatially mismatched. The polarization of light may be designed with focusing of higher order laser modes,[12] phase discontinuity of light,[13] and tunable orbital angular momentum.[14] Nowadays, axially symmetric radially and azimuthally polarized (RP and AP) light have found wide applications in the analysis of molecular orientation and symmetry.[6,15]

Evaluation and control of the near-field polarization state are directly linked to the properties of optical nano-antennas (often referred to as tips) such as their shape, size, and orientation relative to the polarization direction of the incident light. A de-focused imaging technique[16] and a polarization-dependent analysis[17,18] provide the possibility to explicitly determine the direction of dipole oscillation at the tip apex. However, the tip apex polarizability tensor is commonly anisotropic since often it has an elongated shape. This is the main reason why the tip orientation tremendously affects the

[a]*Department of Optics and Nanophotonics, Institute of Physics, Kazan Federal University, Kremlevskaya, 16, Kazan, 420008, Russia. E-mail: skharint@gmail.com, Sergey.Kharintsev@kpfu.ru; Tel: +7(843)2337741*
[b]*Institute of Perspective Technologies, Tatarstan Academy of Sciences, Baumana, 20, Kazan, 420111, Russia*
[c]*Department of Chemistry and Chemical Biology, Harvard University, 12 Oxford Street, Cambridge, MA 02138, USA*
[d]*Department of Theoretical Physics, Institute of Physics, Kazan Federal University, Kremlevskaya, 16, Kazan, 420008, Russia*
[e]*Department of Chemical Engineering, Imperial College, London, SW7 2AZ, UK*

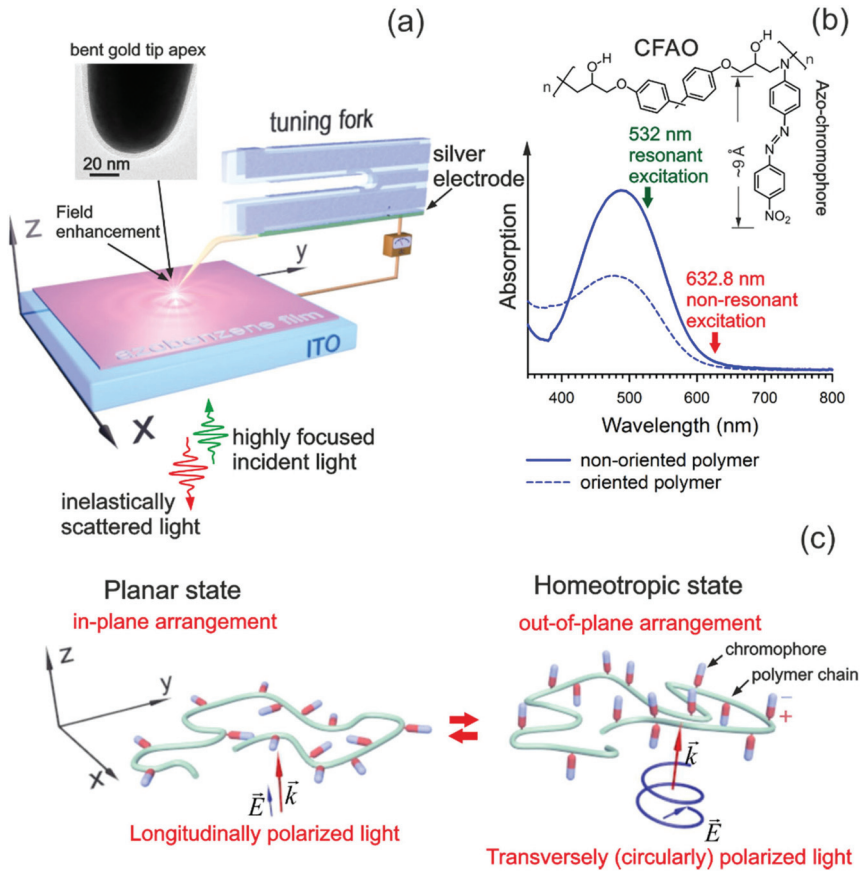

Fig. 1 (a) Schematic diagram of our experimental setup, with a TEM image of the gold tip apex shown as an inset. (b) The chemical structure of a CFAO molecule and its absorption before (solid) and after (dashed) dc electrical poling at above glass temperature. (c) In- and out-of-plane orientation of the azo-dyes with longitudinally and transversely polarized light.

tip–light coupling.[19] It means that an upright tip, that is perfectly smooth and cone-shaped, illuminated with longitudinal light, provides a maximal contribution to the field enhancement, whereas its tilt relative to the light polarization direction inevitably reduces the strength of the coupling.[19] Generally speaking, the conical tips are not suitable for performing polarization-controlled near-field optical microscopy. For this purpose, a spherical nanoparticle-shaped tip apex with isotropic polarizability might be helpful to control the near-field polarization with the incident light in a wide angular range.[18] Unfortunately, the reproducibility of the sphere-like gold tip apexes prepared with electrochemical etching is still low.[20] An alternative approach is to bend the tip, as depicted in Fig. 1(a), in such a way that the in-plane and out-of-plane 'pure' polarizations, perpendicular to each other, contribute to the field enhancement equally. The bent conical gold tip is coupled with the RP and AP light in an optimal way, as demonstrated in ref. 17.

In this paper, we study the planar and homeotropic states of a sub-10 nm thick epoxy-based side-chain azo-polymer film using tip-enhanced Raman scattering (TERS) microscopy[6,21] and contact scanning capacitance microscopy (c-SCM).[22] The enhancement of the TERS intensities depends dramatically on the near-field polarization, as was established earlier for both a radial breathing mode and a graphite mode of single-walled carbon nanotubes.[7,8,11] Inspired by this finding, we introduce near-field Raman dichroism for quantitative analysis of the molecular orientations of the polar azo-moieties in a glassy environment. In our approach, the out-of-plane orientation of the azo-dyes is set with a bias voltage (bv) gold tip, whereas the in-plane alignment is readily achieved with the resonant longitudinal near-field due to orientation angular burning (OAB).[23–28] Non-destructive monitoring of the planar and homeotropic alignments can be probed with transverse and longitudinal non-resonant optical near-fields equally. In addition, we provide evidence for the planar and homeotropic states being robust and stable through probing the local permittivity of the azo-polymer thin film with the s-SCM tool.

2. Results and discussion

2.1. Photo-induced optical anisotropy in azo-polymers at the nanoscale

Fig. 1(a) shows a sketch of an inverted optical system equipped with a scanning probe microscope, which we used in our

experiments. The bent gold tip is attached to a conductive long tab of a horizontally oriented tuning fork. Armed with the near-field polarization analysis,[17] the tilt of the tip in respect to the *z*-direction is estimated to be approximately 42°. A high numerical aperture (NA = 1.49) 100× objective delivers the RP and AP light onto the tip apex to excite a localized surface plasmon in it. Strong focusing of axially symmetric RP and AP laser modes results in the longitudinal and transverse polarization (LP and TP), respectively.[6–12] The azobenzene-functionalized polymeric thin film is produced by spin-casting the polymer bulk onto an indium tin oxide (ITO) substrate that operates as a counter electrode. As a target sample of interest we have used a 4-amino-4′-nitroazobenzene chromophore (Disperse Orange 3) covalently attached to epoxy-based oligomers containing hydroxyl groups, further referred to as CFAO (T_g = 130 °C, M_w = 24 200).[29,30] This material is a promising non-linear optical medium for the second harmonics generation, showing a higher quadratic susceptibility of ~62 pm V^{-1}.[29] A chemical structure of this molecule is shown in Fig. 1(b). One should emphasize that no spacers are used to attach the azo-moiety to the backbone. Therefore, the bulk amorphous polymer cannot exhibit liquid crystalline behavior. A decrease of the thickness of the CFAO thin film down to several nanometers can lead to the rapid arrangement of the azo-chromophores due to their higher mobility. A schematic illustration of the chromophore orientation is given in Fig. 1(c) where the azo-dyes are randomly oriented either in or out of the thin film plane exposed to both longitudinally and transversely polarized light. As follows from Fig. 1(c) the planar and homeotropic states are achieved using resonant LP and TP light due to the OAB effect, respectively. In order to differentiate the two orientational states their non-resonant counterparts are used. Alternatively, the out-of-plane arrangement may be induced by a local dc electrical field that is applied in the *z*-direction. In this case, the film becomes non-centrosymmetric, showing non-zero quadratic susceptibility.

A sub-10 nm thick CFAO film is prepared with spin-casting of the bulk polymer diluted by cyclohexanone in a volume proportion 1 : 100 (Fig. 2(a)), 1 : 150 (Fig. 2(b)), and 1 : 200 (Fig. 2(c)). As a result, we observe a spongy micro-structured thin film with the thickness estimated as the difference between the peaks in the heights histogram, as shown in the insets in Fig. 2. The mean thickness of such films is in the order of 2.3 ± 0.3 nm. A solid thin film can be fabricated with a higher concentration of the polymer, however, its thickness gets inevitably larger. A structure of mesopores containing a polymeric bump at their core is caused by wettability of the polymer with the glass substrate. As follows from the figure, a decrease of the concentration of the polymer leads to an increase of the pore size. Due to the sub-wavelength spatial resolution, appropriate height constant valleys can be found on the ragged film to study orientation effects.

At lower concentrations, for example 1 : 400 or smaller, the pores are degenerated into randomly dispersed polymeric droplets. A dark depletion area is indicative of a CFAO monolayer. To confirm this, we make a straight scratch with a softer

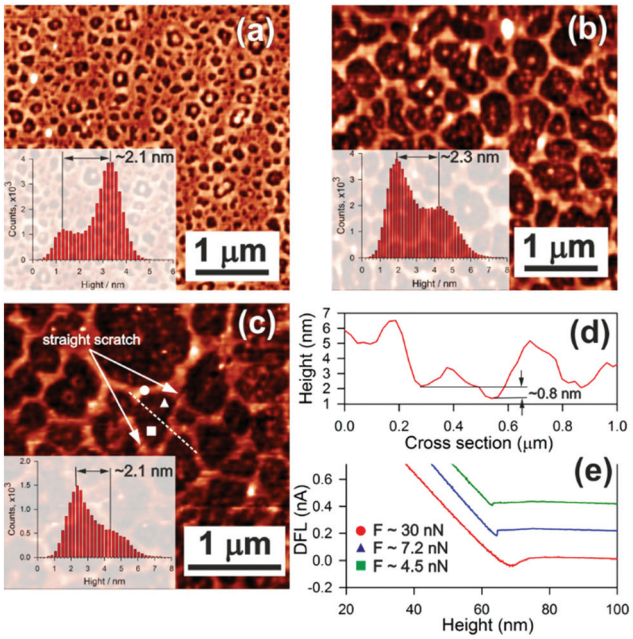

Fig. 2 A CFAO ultrathin film prepared with spin-coating of CFAO solution diluted with cyclohexanone at different volume proportions: 1 : 100 (a), 1 : 150 (b), and 1 : 200 (c). (d) A cross-section along the dashed straight line shown in (c). (e) AFM approach/withdraw curves taken at various spots marked as the circle, square and triangle in (c).

AFM cantilever (0.01 N m^{-1}) in contact mode, as shown in Fig. 2(c). Seeing it again in semi-contact mode reveals a ~0.8 nm sized pitch on the cross-section (Fig. 2(d)) taken along the white dashed straight line in Fig. 2(c). Thus, the thickness of the ragged film is estimated to be approximately 3.5 ± 0.3 nm. In particular, this finding allows the suggestion that the azo-dyes almost certainly lie in the thin film plane to minimize the surface free Gibbs energy. Adhesion forces have been measured with approach/withdrawal curves (Fig. 2(d)) at the points indicated with a circle (on the polymer bulk, 30 nN), a triangle (on the depletion area, 7.2 nN), and a square (on the pitch, 4.5 nN). These results confirm the assumption of the existence of the polymer depletion areas.

The orientation of the azo-chromophores is recognized by means of non-resonant polarization-controlled TERS (PC-TERS) microscopy of a ~4.7 ± 0.3 nm thick CFAO film. An AFM image of the film is given in Fig. 3(a). This figure clearly shows four depletion areas with polymeric bumps at their centers. These bumps are very helpful for assigning an optical response to the topography of the sample. Raman spectra with and without a bent gold tip illuminated with non-resonant 632.8 nm LP and TP light, taken at an arbitrary spot marked with a star, are shown in Fig. 3(b). The intensity of the light at the CFAO film and the exposure time were ~1 kW cm^{-2} and 10 s, respectively. Five-fold and twenty-fold enhancements were reached for longitudinal and transverse excitation. The two characteristic vibrational modes at 1110 cm^{-1} and 1147 cm^{-1} correspond to the Ph-NO_2 stretch and Ph-NN stretch.[31] A peak at 1130 cm^{-1} is negligible, which is commonly responsible for

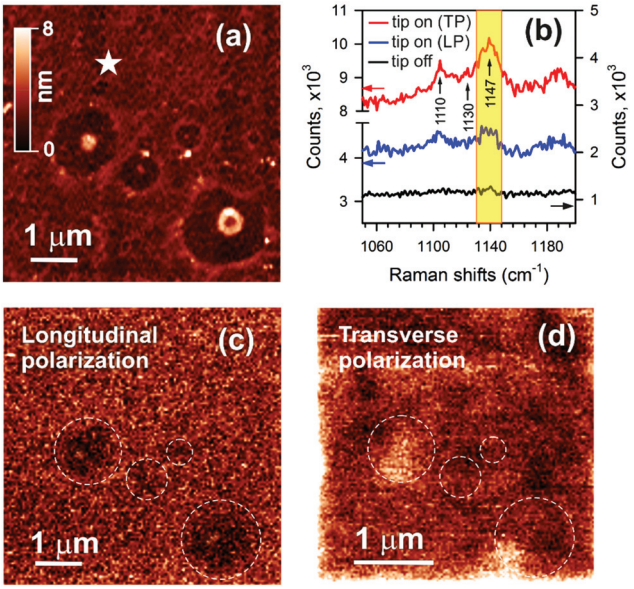

Fig. 3 (a) AFM image of the CFAO thin film; (b) far-field Raman spectrum (black curve) and PC-TERS spectra with TP (red curve) and LP (blue curve); and PC-TERS maps at the 1147 cm^{-1} peak upon LP (c) and TP (d) illumination.

photodegradation of the CFAO thin film in air, as earlier reported.[6] PC-TERS maps at the 1147 cm^{-1} peak for both RP and AP incident light are shown in Fig. 3(c) and (d). A weak Raman contrast with the LP excitation compared to that with the TP excitation is a convincing outcome for the in-plane arrangement of the azo-dyes. Bumps at the center of the depletion areas are unavailable because of the mismatched tip–light coupling upon altering the polarization. With the transverse excitation, the distribution of the intensity over the extent of the thin film is slightly inhomogeneous. Bright Raman responses coming from the bumps are shifted from the centers of the depletion zones due to the above-mentioned reason. It is important to notice that photo-isomerization comes into play when resonant PC-TERS microscopy is in use. Therefore, this instrument is not suitable for reading optical information stored with the chromophore due to the OAB effect.

Along with photo-isomerization, the temperature-dependent mobility of polymeric chains plays a crucial role in the alignment of the azo-dyes.[32–34] At the above glass temperature, the azo-polymer thin film can be easily oriented with a corona discharge-based dc electrical poling.[30] In this case, the pigments are partly aligned out-of-plane towards the z-direction. A specific spectroscopic fingerprint of the ordered state is the appearance of the absorption dichroism in the visible region (for electronic excitations $S_1(n\pi^*)$ and $S_2(\pi\pi^*)$) which can be defined as:

$$D^{ab} = \frac{2I_{\parallel}^{ab} - I_{\perp}^{ab}}{2I_{\parallel}^{ab} + I_{\perp}^{ab}},\ I_{\parallel}^{ab} \equiv {I_z}^{ab} \sim |\mu_{nm}|_z^2,\ I_{\perp}^{ab} \sim |\mu_{nm}|_x^2 + |\mu_{nm}|_y^2, \quad (1)$$

where $\mu_{nm} = \langle m|\hat{\mu}|n\rangle$ is a transition dipole moment between the electronic states $|m\rangle$ and $|n\rangle$. Unlike the traditional formulas for linear or circular dichroism, longitudinal (out-of-plane) absorbance $I_{\parallel}^{ab}$ and transverse (in-plane) absorbance $I_{\perp}^{ab}$ are used in eqn (1).

The absorption dichroism, defined with eqn (1), serves as a quantitative indicator of the transverse and longitudinal orientation. For the isotropic state we have $2I_{\parallel}^{ab} = I_{\perp}^{ab}$ and therefore, $D^{ab} = 0$. In the limiting cases, upon TP and LP light illumination, the dichroism should become −1 and 1, respectively. The change in the sign of this magnitude could be used to encode optical information. However, a direct measurement of the electronic absorption spectra $I_{\parallel}^{ab}$ and $I_{\perp}^{ab}$ results inevitably in the disturbance of the ordered state due to photo-isomerization. Non-resonant Raman spectroscopy and infrared spectroscopy are preferable to delicately probe the induced orientation in a non-destructive fashion. In far-field Raman spectroscopy, a depolarization ratio ρ is normally used to distinguish the molecular symmetry and vibrational modes. However, this magnitude is used for linearly polarized light only. In analogy with eqn (1) we introduce the following expression for near-field Raman dichroism at a vibrational mode ν:

$$D^{R} = \frac{2I_{\parallel}^{R} - I_{\perp}^{R}}{2I_{\parallel}^{R} + I_{\perp}^{R}}, \quad (2)$$

where the transverse $I_{\perp}^{R}$ and longitudinal $I_{\parallel}^{R}$ polarized Raman intensities read as

$$I_{\parallel}^{R} \equiv {I_z}^{R} \sim |\alpha_{nm}|_{zz}^2,\ I_{\perp}^{R} \sim |\alpha_{nm}|_{xx}^2 + |\alpha_{nm}|_{yy}^2,$$

where $(\alpha_{nm})_{ij}$ $(i, j = (x, y, z))$ are matrix elements of dynamic polarizability of the molecule, and the coordinate system is fixed with the z-axis orthogonal to the plane of the film. Because of weak light–matter interaction and phase retardation in the ordering of azo-chromophores in depth, PC-TERS microscopy is necessary to spectroscopically probe the azo-polymer films with sub-wavelength spatial resolution. However, the near-field polarization control is still challenging[16,17] since switching of the polarization of the light leads to the mismatching of the tip apex and the focal spot. With this reason, we suggest rotation of a highly anisotropic rod-like molecule with a local dc electrical field. Instead of eqn (2) we introduce the voltage-dependent near-field Raman dichroism as follows:

$$D^{R}(V) = \frac{I_{\parallel}^{R}(V) - I_{\parallel}^{R}(0)}{I_{\parallel}^{R}(V) + I_{\parallel}^{R}(0)}, \quad (3)$$

where the light $I_{\parallel}^{R}$ is polarized towards the applied electric field, in our case, along the z-direction. One should keep in mind that the initial state of the sample has to be isotropic at $V = 0$. This approach simplifies the foregoing experimental setup (Fig. 1(a)), in which an upright gold conical tip is preferred. Fig. 4(a) shows resonant TERS spectra of the CFAO thin film, obtained with a biased (red dashed curve) and unbiased (blue dashed curve) gold tip. Both the noisy spectra were smoothed with a conventional singular value

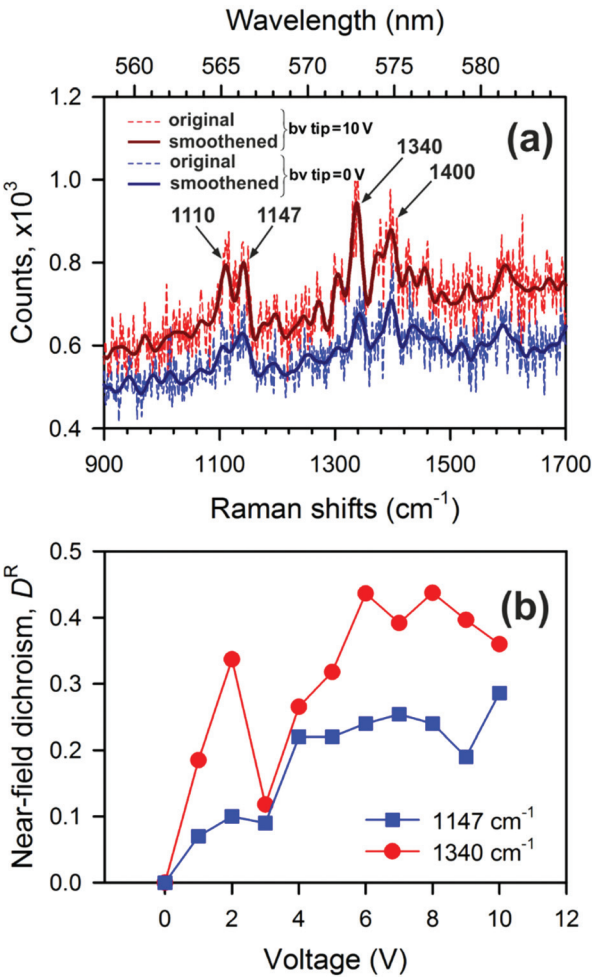

Fig. 4 (a) TERS spectra of the CFAO thin film at different voltages, and (b) dependence of near-field dichroism on applied voltage for two characteristic vibrational modes.

decomposition technique. The Raman spectra enhanced with an unbiased (0 V) and biased (+10 V) tip correspond to the blue solid curve and red solid curve, respectively. We have used the excitation wavelength of 532 nm, which lies within the absorption band, to improve the effect performance due to a reduced fluorescence, a photo-induced heating of the film and, finally, the OAB effect. The power focused on the sample under study and the exposure time were ~1 kW cm^{-2} and 1 s, respectively. The intensities of all peaks are inhomogeneously increased when a voltage of 10 V between the gold tip and the ITO substrate is supplied. Special attention should be paid to the 1340 cm^{-1} peak assigned to the NO_2 symmetric stretch, which is enhanced in comparison with the other Raman peaks. Such behavior is followed by both the anisotropic nature of their Raman tensors and tip-enhanced longitudinal optical fields. Indeed, all strong Raman-active modes of *trans*-azo-chromophores are characterized by single component Raman tensors. For example, the Raman tensors for the vibrational modes of 1147 cm^{-1} and 1340 cm^{-1} of the DO-3 chromophore computed using the time-dependent density functional theory for a 632.8 nm excitation wavelength are:

$$\overleftrightarrow{\alpha}_{1147\,\mathrm{cm}^{-1}} = \begin{bmatrix} 0.00 & 0.00 & 0.00 \\ 0.00 & 0.04 & -0.07 \\ 0.00 & -0.07 & 4.84 \end{bmatrix} \text{ and}$$
$$\overleftrightarrow{\alpha}_{1340\,\mathrm{cm}^{-1}} = \begin{bmatrix} -0.01 & 0.00 & 0.00 \\ 0.00 & 0.04 & 0.01 \\ 0.00 & 0.01 & 6.95 \end{bmatrix} \quad (4)$$

where the numerical values are given in atomic units and the *z*-axis is directed along the chromophore. Despite the fact that these tensors have a similar structure, the changes in Raman intensities are noticeably different, as seen from Fig. 4(a). Moreover, the induced dipole moment $\boldsymbol{\mu}_{\mathrm{ind}}$ is determined as:

$$\boldsymbol{\mu}_{\mathrm{ind}} = \overleftrightarrow{\alpha}_{\mathrm{eff}} \boldsymbol{E}_{\mathrm{inc}}(\omega) \equiv [\overleftrightarrow{\alpha}^{\mathrm{mol}} + \overleftrightarrow{\alpha}^{\mathrm{tip}} \cdot g] \boldsymbol{E}_{\mathrm{inc}}(\omega), \quad (5)$$

where $\overleftrightarrow{\alpha}^{\mathrm{mol}}$ and $\overleftrightarrow{\alpha}^{\mathrm{tip}}$ present a frequency-dependent molecule polarizability without and with a gold tip, g is an enhancement factor, and $\boldsymbol{E}_{\mathrm{inc}}(\omega)$ is an oscillating optical field. $\boldsymbol{\mu}_{\mathrm{ind}}$ is dependent on the properties of the gold tip and its orientation in respect to the molecule frame. Obviously, at $g \gg 1$ a significant contribution to the Raman tensor is made with the tip-dependent molecule polarizability. Since the form of this tensor is in general not known, an understanding of no photobleaching at high intensity optical fields is still unavailable. It follows from the behavior of intensities peaked at 1340 cm^{-1} and 1400 cm^{-1} (NN symmetric stretch), which increase with the voltage rather than drop.[22]

Thus, the longitudinal and transverse optical anisotropy of the CFAO polymer thin film exposed to optical and electrical fields at the nanoscale can be quantitatively characterized with the near-field Raman dichroism $D^{\mathrm{R}}(V)$. Fig. 4(b) demonstrates a dependence of this magnitude *versus* the applied voltage for two characteristic vibrational modes. It also follows from the figure that the Raman dichroism for both peaks is saturated for voltages of above 5 V. It means that most of the azo-dyes are oriented out-of-plane and further increasing the voltage does not affect the homeotropic state. Furthermore, when the voltage is returned to zero, the Raman spectrum is reversibly restored under resonant illumination. In the dark, the oriented state retains its form for as long as several hours. This state can be safely unravelled with non-resonant near-fields. Closing this section, we conclude that control of the near-field polarization in TERS microscopy is of great advantage, as it allows one to probe the highly directional intrinsic properties of the azo-dyes within a glassy environment at the nanoscale. In the context of optical near-field memory this instrument may provide not only ultrahigh density data storage but contributes to error correction and polarization multiplexing.[1]

2.2. Nanoscale probing of the orientation of azo-chromophores with scanning capacitance microscopy

The orientation of the azo-chromophores under dc electrical and optical poling results in the occurrence of a surface potential due to negatively charged NO_2 tails. As was demonstrated

earlier in ref. 6, the Kelvin probe method allows one to locally probe the surface potential with nanometer scale accuracy. However, by supplying a dc electrical field in the tip–sample system, the CFAO thin film surface becomes charged not only because of the orientation of the azo-dyes but also because of an ionic injection mechanism. As a result, the external charges are exponentially relaxed and the net induced potential vanishes.[6] A direct measurement of the permittivity of the oriented thin film with c-SCM allows the injection effect to be reduced substantially so that its contribution becomes almost negligible. Despite the fact that c-SCM is one of the most common tools for analyzing doping profiles in semiconductor-based structures, it is a promising non-destructive tool to unravel the local molecular anisotropy based on a dielectric response of azobenzene-functionalized amorphous and liquid crystal polymers. As a result, stored charges in an insulator layer of the metal–insulator–semiconductor (MIS) heterostructure are easily recognized.

Fig. 5(a) shows the sketch of the experimental setup for measuring the capacitance of the CFAO thin film. In our experiment, we intend to qualitatively estimate the capacitance $C(V)$ + const, which is very sensitive to the surface topography. Fig. 5(b), (e), (j), (c), (f), and (h) show the topography and capacitance of the CFAO thin films at different bias voltages ($V_{dc} = V_{tip} - V_{sample}$). In assumption of a plane capacitor, the permittivity may be evaluated as a product of the topography and capacitance maps, as given in Fig. 5(d), (g), and (k). At zero bias, we observe the inhomogeneous distribution of the pigments in the thicker polymer. In the case of $V_{dc} = -10$ V a permittivity contrast is noticeably enhanced. It means that all azo-chromophores are anchored along the electric field direction with negatively charged NO_2 ends that are oriented upward. In other words, longitudinal optical anisotropy takes place. Fig. 5(l) shows the heights histogram before (red curve) and after (blue curve) applying the dc electric field. We observe that the mean height of the polymeric structure increases by a magnitude of ~0.7 nm, that is, approximately one chromophore in length. This state, generated with the dc electric field in the ultrathin film at room temperature, is stored for several hours. One should notice that the orientation polarization of the azo-dyes within thicker films drops enough rapidly. For example, a 100 nm thick polymer film holds the homeotropic state for 1–2 min only.[6] Cross-sections taken along dashed straight lines provide evidence that the azo-chromophores are more easily oriented in the vicinity of interfacial features rather than in thicker fragments of the polymer. In particular, a crater-like peculiarity is formed on the surface of the polymeric fragment (Fig. 5(m)).

In the case of $V_{dc} = +10$ V the permittivity contrast vanishes. This is explained by the in-plane arrangement of the azo-chromophores, since they cannot follow the electrical field because of the substrate. It gives rise to the transverse anisotropy, by which all chromophores are randomly dispersed in the film plane. Thus, changing the polarity of the applied voltage allows us to handle the oriented states between the planar and homeotropic arrangement of the azo-dyes.

The surface charge that occurs is followed by out-of-plane alignment of the azo-moieties with negatively charged ends

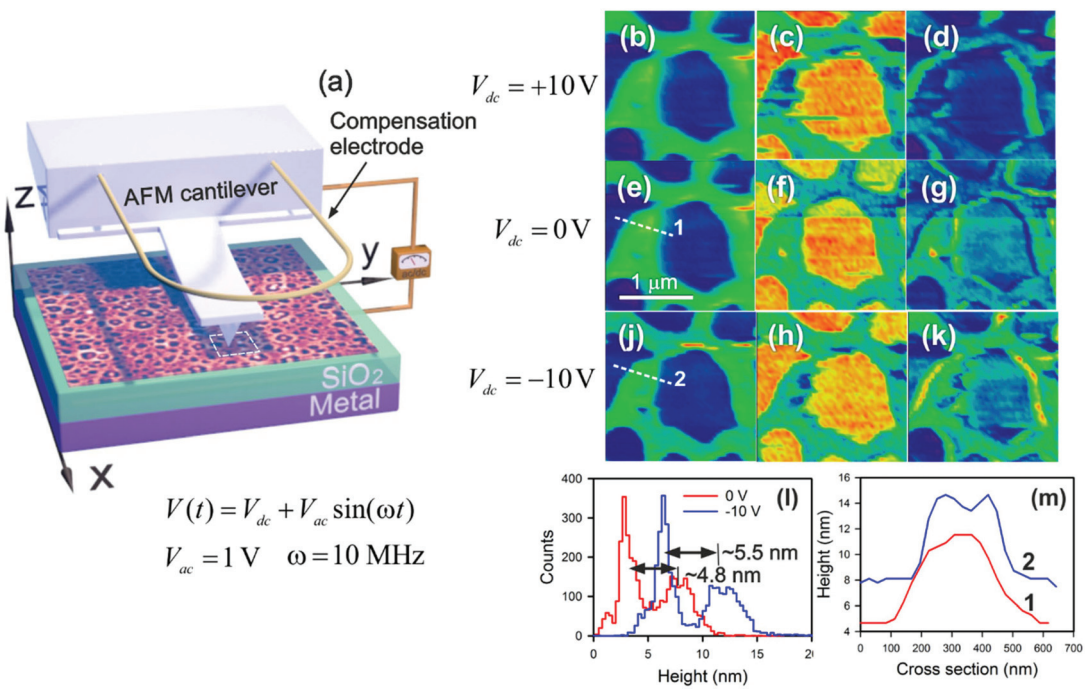

Fig. 5 (a) Sketch of the experimental setup for measuring a local capacity, (b), (e), and (j) AFM images of the CFAO thin film at different dc voltages, (c), (f), and (h) capacity maps of the CFAO thin film at different dc voltages, (d), (g), and (k) a product of AFM images and capacity maps at different dc voltages, (l) a histogram of AFM heights from (e) and (j), and (m) cross-sections along the dashed straight lines in (e) and (j).

going upward. One should bear in mind that the positively charged end group is at load, whereas the other one is free to move (Fig. 1(c)). The induced potential is dependent on the dipole moment of the azo-dyes and their concentration. Therefore, changes in the net surface potential $\Delta\varphi$, according to the Helmholtz equation,[35,36] read as:

$$\Delta\varphi = \frac{N\mu}{\varepsilon_{\mathrm{pol}}\varepsilon_0}\cos(\theta), \quad (6)$$

where N is the density of azo-chromophores, μ is the dipole moment, θ is the average tilt angle of the dipole with respect to the surface normal, $\varepsilon_{\mathrm{pol}}$ is the relative permittivity of the CFAO polymer, and ε_0 is the permittivity of a vacuum.

Several important properties of the polar polymer thin film, such as the order and dipole depolarization, can be derived from eqn (6).[35] Each azo-dye can be considered as an individual local dipole that contributes into the surface potential enhancement. If the azo-dyes concentration is low then the dipoles are located far from each other. Such a system tends to a disordered state and the surface potential vanishes in time. Increasing the azo-dye density in a glassy environment can lead to the depolarization effect and the resulting dipole moment becomes negligible. However, in an ordered polymer ultrathin film with a high concentration of the pigments a cooperative molecular effect[35] comes into play due to a dipole–dipole interaction.

3. Conclusions

In summary, we conclude that a reversible transition between the planar and homeotropic orientation of the azo-chromophores in the sub-10 nm CFAO film can be performed with a hybrid method. The longitudinal optical anisotropy comes with a local dc electric field, whereas the transverse anisotropy is induced with localized longitudinal resonant excitation. This approach potentially can provide access to a single chromophore to store optical information. Thus, the amorphous side-chain azo-polymer thin film may serve as an emerging medium for optical switching and storage. PC-TERS empowers us to both encode and decipher in-plane and out-of-plane phase states with sub-wavelength spatial resolution. Importantly, a bent gold tip provides equal contributions to the field enhancement with transverse and longitudinal optical near-fields regardless of the polarization of incident far-fields. Nanoscale quantitative analysis of the polarization orientation can be performed by measuring the near-field Raman dichroism. We have demonstrated changes in the near-field Raman dichroism for different molecular orientations of the pigments driven by the applied voltage. The use of this parameter requires more theoretical work to provide further insights into the mechanism of TERS. The in- and out-of-plane orientation of the azo-polymer thin film that is exposed to a dc electric field is visualized by means of a local permittivity registered with the c-SCM instrument. The stability of the polar homeotropic phase of the CFAO thin film exposed to a dc electric field may be caused by the dipole–dipole interaction between the azo-dyes within the sub-10 nm polymer film provided that they contain a high concentration of the pigments. This state holds during several hours. It is important to notice that the ordering state of the azo-dyes is strongly sensitive to the mobility of polymeric groups and backbones. In other words, α,β,γ-transitions in polymers play a crucial role in holding side-chains oriented. However, with a decreasing film thickness, the glass transition temperature (α-transition) may drop considerably.[37] Due to interfacial interactions, the glass transition temperature is dependent on a substrate and its choice is of great importance for stability of the oriented thin film. Finally, we suggest that the results of this study will be helpful to develop the next generation of non-volatile reversible near-field optical memory materials, as an emerging prospective candidate for future big data storage.

4. Methods

4.1. Sample preparation

A 4-amino-4′-nitroazobenzene chromophore covalently attached to the polymer backbone of epoxy-based oligomers containing hydroxyl groups (CFAO) was synthesized by M. Balakina's research group[29,30] and helpfully brought to us for experimental study. A solution was prepared by dissolving 7 wt% CFAO compound in 1 mL cyclohexanone. To control the film thickness we diluted the bulky polymer with cyclohexanone in volume proportions as indicated in the text. The thin film was produced by means of spin-coating ~1 μL CFAO solution onto an ITO/glass substrate at a rotation rate of 12 000 rpm for 3 min. In order to eliminate remaining solvent the thin film was annealed at the glass temperature of 130 °C and 10 mbar for 2 h.

4.2. Gold tip preparation

TERS-active gold tips were fabricated from a 100 μm gold wire (purity 99.99%, Goodfellow) immersed in a mixture of fuming hydrochloric acid (HCl, 37%), isopropanol ($CH_3CH(OH)CH_3$, 96%) and distilled water in a volume proportion of 0.5 : 0.3 : 0.2, by means of dc-pulsed voltage electrochemical etching with a self-tuneable duty cycle and working potentials of V_b = 1.5 V and V_{up} = 1.9 V.[38] With that, ~20 nm curvature radius gold tips were obtained (inset in Fig. 1(a)). Once prepared, the probes were thoroughly rinsed with distilled water and dried with nitrogen. After that, they were under mechanical load to become bent and glued to a conductive long tab of a horizontally oriented tuning fork (TF103_NTF, NT-MDT) operating at a resonance frequency of ~192 kHz, as shown in Fig. 1(a). Approaching the gold tip to a thin film was safely performed with the help of a normal force feedback scheme with a scanning head (SNLG103NTF, NT-MDT) at a set-point value as small as ~95%.

4.3. TERS measurements

All transmission mode TERS spectra and near-field imaging are measured with scanning probe microscopy (SPM) equipped

with a Raman spectrometer NTEGRA SPECTRA™ (NT-MDT, Russia). A 100× oil immersion objective (Olympus, NA = 1.49, refractive index n = 1.516) delivers light with excitation wavelengths of 532 nm an 632.8 nm onto the CFAO thin film with a power at the sample of ~1 kW cm^{-2}. The light polarization is designed with a S-waveplate, linear-to-radial/azimuthal polarization converter (Altechna, Lithuania). The bent gold tip is coupled to the highly squeezed light by monitoring a two-lobe Rayleigh scattering pattern that is rotated with the linear polarization around the optical z-axis. Importantly, this optical pattern is blurred because of the tip tilt in respect to the z-axis. For radially and azimuthally polarized light, a recently developed polarization technique was utilized.[17] 128 × 128 pixel reflection and near-field spectroscopic images were raster scanned with a step of 20 nm and an exposure time per pixel of 0.1 s and, finally, captured with a photomultiplier (Hamamatsu, Japan) and a Newton EMCCD camera (ANDOR, Ireland) cooled down to −100 °C. A spectral resolution of the order of 3 cm^{-1} was achieved with 600 grooves per mm grating. Also, the hybrid SPM-equipped Raman spectrometer is applied for measuring the topography, phase contrast, and capacitance with nanometer scale accuracy.

4.4. Capacitance measurements

As mentioned above, the capacitance $C(V)$ + const of the CFAO ultrathin films was qualitatively evaluated with the NTEGRA SPECTRA equipped with a unique contact scanning capacitance microscopy (c-SCM) unit (AU030, NT-MDT) and a measuring head (SF005NTF, NT-MDT), as outlined in Fig. 5(a). It is well-established that the capacitance-based image contrast suffers extremely from the induced stray capacitance (~1 pF) exceeding the tip–sample capacitance (~1 aF) by several orders of magnitude.[22] This drawback is successfully eliminated by both electromechanical correction with a semi-ring compensation electrode and electrical balancing. Thus, the tip–sample capacitance becomes available to be reliably measured. The remnant stray capacitance disappears utterly when measuring dC/dV rather than $C(V)$ + const. One should keep in mind that the determination of an absolute value of the capacitance and its derivatives are still challenging. A rigorous analytical theory for calculating the capacitance between the metallic tip and the MIS structure has been developed by Ruda and Shik.[22] A stray capacitance of ~100 aF, referred to as the const, remains in the tip–sample system while scanning. A 10 MHz voltage signal with an amplitude of 1 V was applied to the sample with different dc voltages of −10 V, 0 V, and +10 V. For measurement purposes, we used specialized AFM cantilevers (CSG10-Pt, NT-MDT) with a resonant frequency of ~14–18 kHz and a force constant of ~0.03–0.2 N m^{-1}.

4.5. Raman tensors calculations

The Raman tensors of the azo-chromophore were computed using a quantum chemistry package Turbomole, version 6.0.[39] The molecular geometries were optimized with the B3LYP hybrid functional[40] and the triple-ζ valence-polarization basis sets def2-TZVP.[41] The permittivity of the polymer host was accounted for using the COSMO model with the effective dielectric constant ε_{pol} = 4.8.

Conflict of interest

The authors declare no competing financial interest.

Acknowledgements

This work was financially supported by the Russian Foundation for Basic Research (no. 15-42-02339). We are grateful to Prof. M. Yu. Balakhina (A. E. Arbuzov Institute of Organic and Physical Chemistry KSC RAS) for preparing samples and acknowledge the help from A. Shelaev (NT-MDT), A. V. Kharitonov (Kazan Federal University), A. R. Gazizov (Kazan Federal University) and D. Rappoport (Harvard University) for invaluable and fruitful discussions. This work was done using equipment of Federal Center of Shared Equipment of Kazan Federal University. S. K. S. also acknowledges the support from the subsidy allocated to Kazan Federal University for performing the state assignment in the area of scientific activities.

Notes and references

1 M. Gu, X. Li and Y. Cao, *Light: Sci. Appl.*, 2014, **3**(5), e177.
2 H. Li, J. Wang, H. Lin, L. Xu, W. Xu, R. Wang, Y. Song and D. Zhu, *Adv. Mater.*, 2010, **22**, 1237–1241.
3 T. Ikeda and O. Tsutsumi, *Science*, 1995, **268**(5219), 1873–1875.
4 H.-S. P. Wong, S. Raoux, S. Kim, J. Liang, J. P. Reifenberg, B. Rajendran, M. Asheghi and K. E. Goodson, *Proc. IEEE*, 2010, **98**(12), 2201–2227.
5 K. Ogawa, *Appl. Sci.*, 2014, **4**, 1–18.
6 S. S. Kharintsev, A. I. Fishman, S. G. Kazarian, I. R. Gabitov and M. Kh. Salakhov, *ACS Photonics*, 2014, **1**, 1025–1032.
7 Y. Saito and P. Verma, *J. Phys. Chem. Lett.*, 2012, **3**(10), 1295–1300.
8 Y. Saito, N. Hayazawa, H. Kataura, T. Murakami, K. Tsukagoshi, Y. Inouye and S. Kawata, *Chem. Phys. Lett.*, 2005, **410**, 136–141.
9 N. Hayazawa, Y. Saito and S. Kawata, *Appl. Phys. Lett.*, 2004, **85**, 6239–6241.
10 Y. Gilbert, R. Bachelot, P. Royer, A. Bouhelier, G. P. Wiederrecht and L. Novotny, *Opt. Lett.*, 2006, **31**(5), 613.
11 T. Mino, Y. Saito, H. Yoshida, S. Kawata and P. Verma, *J. Raman Spectrosc.*, 2012, **43**(12), 2029–2034.
12 L. Novotny and B. Hecht, *Principle of Nano-Optics*, Cambridge University Press, 2012, p. 539.
13 N. Yu, P. Genevet, M. A. Kats, F. Aieta, J.-P. Tetienne, F. Capasso and Z. Gaburro, *Science*, 2011, **334**(6054), 333–337.

14 I. M. Gecevič, R. Drevinskas, M. Beresna and P. G. Kazansky, *Appl. Phys. Lett.*, 2014, **104**(23), 231110.
15 L. Novotny, M. Beversluis, K. Youngworth and T. Brown, *Phys. Rev. Lett.*, 2001, **86**(23), 5251–5254.
16 T. Mino, Y. Saito and P. Verma, *ACS Nano*, 2014, **8**(10), 10187–10195.
17 S. S. Kharintsev, A. I. Fishman, S. G. Kazarian and M. K. Salakhov, *Phys. Rev. B: Condens. Matter Mater. Phys.*, 2015, **92**(11), 115113.
18 T. Mino, Y. Saito and P. Verma, *Appl. Phys. Lett.*, 2016, **109**, 041105.
19 R. V. Maximiano, R. Beams, L. Novotny, A. Jorio and L. G. Cancëado, *Phys. Rev. B: Condens. Matter*, 2012, **85**, 235434.
20 S. S. Kharintsev, G. G. Hoffmann, A. I. Fishman and M. Kh. Salakhov, *J. Phys. D: Appl. Phys.*, 2013, **46**(14), 145501.
21 R. M. Stöckle, Y. D. Suh, V. Deckert and R. Zenobi, *Chem. Phys. Lett.*, 2000, **318**, 131–136.
22 A. Shik and H. E. Ruda, *Surf. Sci.*, 2003, **532**, 1132–1135.
23 R. H. El. Halabieh, O. Mermut and C. J. Barrett, *Pure Appl. Chem.*, 2004, **76**, 1445–1465.
24 Z. Mahimwalla, K. G. Yager, J. Mamiya, A. Shishido, A. Priimagi and C. J. Barrett, *Polym. Bull.*, 2012, **69**(8), 967–1006.
25 Z. Sekkat, M. Buchel, H. Orendi, H. Menzel and W. Knoll, *Chem. Phys. Lett.*, 1994, **220**(6), 497–501.
26 P. Lefin and C. Fiorini, *Pure Appl. Opt.*, 1998, **9**, 323–328.
27 C. Cojocariu and P. Rochon, *Pure Appl. Chem.*, 2004, **76**, 1479–1497.
28 C. Sourisseau, *Chem. Rev.*, 2004, **104**, 3851–3891.
29 N. A. Nikonorova, M. Y. Balakina, O. D. Fominykh, M. S. Pudovkin, T. A. Vakhonina, R. Diaz-Calleja and A. V. Yakimansky, *Chem. Phys. Lett.*, 2012, **552**, 114–121.
30 T. A. Vakhonina, S. M. Sharipova, N. V. Ivanova, O. D. Fominykh, N. N. Smirnov, A. V. Yakimansky, M. Y. Balakina and O. G. Sinyashin, *Mendeleev Commun.*, 2011, **21**, 75–76.
31 A. M. Nowak and R. L. McCreery, Spectroscopy, *Anal. Chem.*, 2004, **76**, 1089–1097.
32 X. Meng, A. Natansohn, C. Barrett and P. Rochon, *Macromolecules*, 1996, **29**, 946–952.
33 J. Kumar, L. Li, X. L. Jiang, D.-Y. Kim, T. S. Lee and S. Tripathy, *Appl. Phys. Lett.*, 1998, **72**(17), 2096.
34 C. J. Barrett, P. L. Rochon and A. L. Natansohn, *J. Chem. Phys.*, 1998, **109**(4), 1505.
35 A. Natan, Y. Zidon, Y. Shapira and L. Kronik, *Phys. Rev. B: Condens. Matter Mater. Phys.*, 2006, **73**(19), 1–4.
36 R. Sfez, N. Peor and S. Yitzchaik, *J. Phys. Chem. C*, 2010, **114**, 20531–20538.
37 H. Liem, J. Cabanillas-Gonzalez, P. Etchegoin and D. D. C. Bradley, *J. Phys.: Condens. Matter*, 2004, **16**(6), 721–728.
38 S. S. Kharintsev, A. M. Alekseev and J. Loos, *Spectrochim. Acta, Part A*, 2017, **171**, 139–143.
39 R. Ahlrichs, M. Bär, M. Häser, H. Horn and C. Kölmel, *Chem. Phys. Lett.*, 1989, **162**(3), 165–169.
40 A. D. Becke, *J. Chem. Phys.*, 1993, **98**(7), 5648.
41 F. Weigend and R. Ahlrichs, *Phys. Chem. Chem. Phys.*, 2005, **7**(18), 3297–3305.